Progress In Electromagnetics Research, Vol. 110, 403–419, 2010

COMPARISON OF UWB SHORT-PULSE AND STEPPED-FREQUENCY RADAR SYSTEMS FOR IMAGING THROUGH BARRIERS

B. R. Crowgey, E. J. Rothwell, and L. C. Kempel

Department of Electrical and Computer Engineering
Michigan State University, East Lansing, MI 48824, USA

E. L. Mokole

Naval Research Laboratory
4555 Overlook Avenue S. W., Washington DC 20375, USA

Abstract—A canonical problem is used to investigate the effects of various radar parameters on the performance of both stepped-frequency and short-pulse through-barrier radar imaging systems. For simplicity, a two-dimensional problem is considered, consisting of a perfectly conducting strip located behind a lossy dielectric slab of infinite extent illuminated by line sources. To assess the impact of the parameters on system performance, radar received images of the target are created using the reflected field computed at several positions in front of the barrier and adjacent to the sources. Specific radar parameters considered include sample rate, A/D bit length, pulse width, and target SNR for a time-domain system. For a stepped-frequency system, A/D bit length, bandwidth, and target SNR are considered.

1. INTRODUCTION

Through-barrier imaging systems represent an emerging technology with many military and civilian applications, such as disaster response and search and rescue. Several studies have been conducted using various types of imaging systems to assess the potential for detecting people or objects located behind different kinds of barriers [1, 2]. Ultra-wide band (UWB) radars are particularly appealing due to their

Received 13 September 2010, Accepted 17 November 2010, Scheduled 26 November 2010
Corresponding author: Edward J. Rothwell (rothwell@egr.msu.edu).

penetration ability and their capability for resolving small targets [3–7]. These types of radars have already proved their usefulness in synthetic aperture radar (SAR) imaging, ground penetration imaging, and terrain profiling [8–13].

UWB radars may be implemented as either time-domain (short-pulse) or stepped-frequency systems. A time-domain system is typically implemented by transmitting one or more RF cycles and then digitizing the received signal with the use of a high-speed analog-to-digital (A/D) converter [14], although some newer systems employ linear frequency modulation. In a frequency-domain system, a stepped-frequency narrow-band transmitter and receiver are used [15]. Each type of system has its unique advantages and disadvantages. Perhaps the most compelling reason for the predominance of stepped-frequency through-barrier radars are their cheaper cost and easier implementation in comparison to time-domain systems. However, while generally more stable, a stepped-frequency system needs a higher dynamic range, requires a longer acquisition time, and suffers from positional aliasing ("ghosting"). Time-domain systems can produce an image from a single rapid measurement but require high-speed A/D converters to support system bandwidth. These systems are potentially more sensitive to radio frequency interference (RFI). Furthermore, in a low signal-to-noise ratio (SNR) environment, time-domain systems may require the averaging of repeated measurements to improve the SNR, thus increasing the actual acquisition time. In their favor, time-domain systems are able to gate out large-amplitude clutter and to tolerate time-limited saturation by such things as transmitter coupling. Also, the gating function can permit the use of less dynamic range in the receiver.

Each UWB radar system has a particular set of operational parameters that must be chosen properly to produce a useful image. In this paper, detailed analyses of both short-pulse and stepped-frequency UWB radar systems are undertaken to determine the values of radar parameters that are needed to image an object behind a typical barrier successfully. Factors such as pulse width, sampling interval, number of A/D bits, and SNR are examined for the time-domain system, while frequency-domain bandwidth, sampling interval, SNR, and number of A/D bits are examined for the stepped-frequency system.

The required signal-to-noise ratio is particularly important since the maximum detection range for a given target is determined by SNR. The total energy on a target can be increased not only by using frequency-modulation or stepped-frequency approaches, it can also be increased by summing multiple time-domain pulses (averaging). Fortunately, the through-barrier imaging problem presents a short-

range radar scenario where extremely high repetition rates with low peak transmit powers can be used by a time-domain system. Therefore, the present analysis assumes that the final target signal-to-noise ratios for the two types of systems under consideration, stepped-frequency and time-domain, are effectively the same and that other issues like dynamic range dominate. Consequently, comparing the power budgets of the two systems is not germane to this analysis.

By using a simple two-dimensional canonical problem consisting of a conducting strip target located behind a lossy dielectric slab barrier, the desired parameters can be easily altered and their effect on the quality of the resulting radar image can be quantified. Excitation is provided by an array of line sources arranged on the opposite side of the barrier from the target. The field scattered by each line source in turn is computed in the frequency domain and is sampled at multiple positions and at a set frequency interval within a chosen band. This data is used to form an image using an SAR approach and a simple scattering-center technique [16–18]. Data for studying the performance of a time-domain radar is obtained by computing the inverse Fourier transform of finely sampled frequency-domain data. Because a direct correlation between image quality and system parameters is desired, an image radius is defined to quantify the quality of the image. Standard radar measures of target resolvability, such as downrange and crossrange resolution, are avoided due to the difficulty of including the effects of near-zone illumination and the spatial and temporal dispersion of the transmitted pulse that is introduced by the lossy barrier.

2. THE CANONICAL PROBLEM

The canonical problem for the radar parameter study consists of an infinite, lossy, dielectric slab of permittivity $\epsilon = \epsilon_0(\epsilon_r - j\frac{\sigma}{\omega\epsilon_0})$, occupying the region $0 \leq z \leq z_w$, and a thin, perfectly-conducting strip target of width W located at a position $z = z_s$ behind the barrier, as shown in Figure 1. An infinitely long electric line source with current density $\vec{J} = \hat{x}I\delta(z - z_s)\delta(y)$ is located on the z-axis a height z_s above the slab, providing an electric excitation field perpendicular to the y-z plane (TE illumination).

The scattered electric field may be found by solving an electric-field integral equation (EFIE) obtained from applying the boundary condition of zero tangential electric field on the surface of the conducting strip target. Since the total field is the sum of the incident and scattered fields, it is first necessary to find the incident field on the strip, which is the excitation field without the target present. Consequently, the incident field is the electric field in the region below

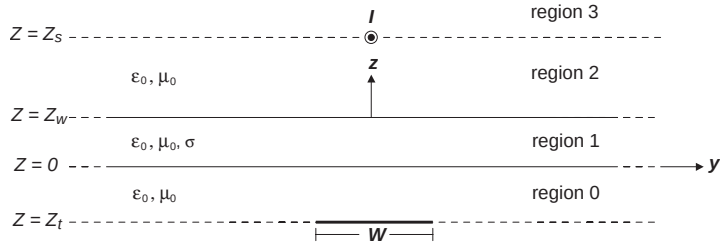

Figure 1. Geometry of the canonical problem showing a line source above a lossy barrier (region 1) with a PEC strip target below the barrier.

the slab produced by a line source above the slab. This field is most easily computed using a two-dimensional Fourier-transform approach and writing the fields in terms of the vector potential $\vec{A} = \hat{x}A_x$.

Consider the canonical problem without the conducting strip. The vector potential in each of the four regions of Figure 1 can be represented using the spatial Fourier transform pairs

$$\vec{\tilde{A}}(k_y, z) = \int_{-\infty}^{\infty} \vec{A}(y, z) e^{-jk_y y} dy, \tag{1}$$

$$\vec{A}(y, z) = \frac{1}{2\pi} \int_{-\infty}^{\infty} \vec{\tilde{A}}(k_y, z) e^{jk_y y} dk_y. \tag{2}$$

Here the time convention $e^{j\omega t}$ is used.

Applying the boundary conditions on tangential $\vec{E}$ and $\vec{H}$ at each of the boundaries and solving for the appropriate potential amplitudes as in [19] yield a formula for the transform of the vector potential

$$\tilde{A}_x(k_y, z) = \frac{I\mu_0}{2jp} e^{-jp|z-z_s|} + \frac{I\mu_0}{2jp} e^{-jp(z+z_s)} e^{2jpz_w} R_\perp, \tag{3}$$

for points $z \geq t$ (source side of the slab). Here

$$R_\perp = \frac{\frac{-p^2}{q} \sin qz_w + q \sin qz_w}{\frac{-p^2}{q} \sin qz_w + 2jp \cos qz_w - q \sin qz_w} \tag{4}$$

is the slab reflection coefficient. For $z < 0$ (the target side of the slab), the vector potential is

$$\tilde{A}_x(k_y, z) = \frac{I\mu_0 e^{jpz} e^{-jp(z_s - z_w)}}{-\frac{p^2}{q} \sin qz_w + 2jp \cos qz_w - q \sin qz_w}. \tag{5}$$

In (3) the first term is the direct potential from the line source and the second term is the potential reflected from the slab, while (5) provides the expression for the transmitted potential. The quantities p and q are the z-directed wave numbers in free space and in the dielectric slab, respectively, and are given by $p = \pm\sqrt{k_0^2 - k_y^2}$ and $q = \pm\sqrt{k^2 - k_y^2}$, where $k_0 = \omega\sqrt{\mu_0\epsilon_0}$ and $k = \omega\sqrt{\mu_0\epsilon}$. The signs on p and q are chosen such that the waves decay as they propagate.

Implementing the inverse Fourier transform and using $\vec{E} = -j\omega\vec{A}$ produce the direct and scattered electric fields

$$E_x(y,z) = \frac{-I\mu_0\omega}{4\pi}\int\limits_{-\infty}^{\infty}\frac{e^{jk_y y}}{p}\left[e^{-jp|z-z_s|} + e^{-jp(z+z_s-2z_w)}R_\perp\right]dk_y, \quad (6)$$

on the source side of the slab ($z \geq t$). The scattered electric field on the target side of the slab ($z < 0$) is

$$E_x(y,z) = \frac{-j\omega I\mu_0}{2\pi}\int\limits_{-\infty}^{\infty}\frac{I\mu_0 e^{jp(z-z_s+z_w)}e^{jk_y y}}{-\frac{p^2}{q}\sin qz_w + 2jp\cos qz_w - q\sin qz_w}dk_y. \quad (7)$$

By using the impressed field on the target side of the slab, an EFIE is formulated for the current on the strip, which is then solved using the method of moments with pulse function expansion and point matching. With this current, the total field on the source side of the slab, consisting of the direct field, the reflected excitation field, and the field scattered by the strip, is computed using (6) as a Green's function to determine the direct and reflected fields and using (7) as a Green's function to determine the scattered field. This total field is the field at the receiving antenna.

3. NUMERICAL VALIDATION

To simulate a SAR, the line source, representing the transmitter, is placed at a chosen horizontal position, and the scattered field is computed at an adjacent point, representing the position of a receiver. The z-positions of the transmitter and receiver are taken to be identical. The transmit/receive pairs are moved parallel to the barrier, and the fields are computed for each pair in the band from 20 MHz to 16 GHz at 20 MHz increments. Since the images are formed in the time domain, the FFT is used to transform the data. Before transformation, the frequency-domain data is multiplied by a windowing function $W(f)$

to remove edge effects. By choosing the windowing function Fourier pair $w(t) \leftrightarrow W(f)$ with

$$w(t) = e^{-\pi(t/T)^2} \cos(2\pi f_0 t) \tag{8}$$

and

$$W(f) = e^{-[T(f-f_0)]^2} + e^{-[T(f+f_0)]^2}, \tag{9}$$

the side lobes in the resulting time-domain data are reduced. Here f_0 is the center frequency of the window function. Note that the inverse transform of the window function, which is a Gaussian-pulse modulated cosine waveform, has an envelope half-amplitude width of T. Thus, the half-amplitude bandwidth of the windowed data is given by

$$\Omega = \frac{4 \ln 2}{\pi T}, \tag{10}$$

and the fractional bandwidth is Ω / f_0 [20].

A typical result is shown in Figure 2(a), where the material parameters of the barrier are taken to be $\epsilon_r = 6$ and $\sigma = 0.001\,\mathrm{S/m}$, which are representative of concrete [21]. In this and all subsequent results, a monostatic radar is simulated where the horizontal positions of the source and observation points are taken to coincide, representing a single transmit/receive antenna. This requires that the direct field be suppressed by excluding the first term in the integrand of (6). To obtain the time-domain waveforms, window parameters $T = 0.05\,\mathrm{ns}$ and $f_0 = 0\,\mathrm{GHz}$ were used, producing an incident time-domain field

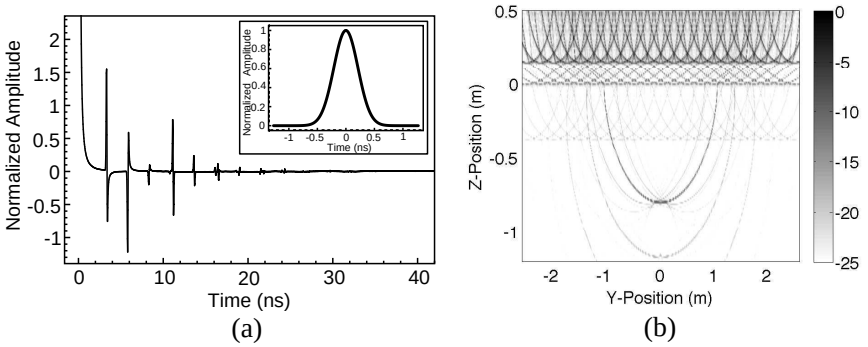

Figure 2. (a) Time-domain total field at a point centered above the conducting strip; (b) Image (scale in dB) of lossy dielectric slab and conducting strip. $z_s = 50\,\mathrm{cm}$, $z_t = 80\,\mathrm{cm}$, $z_w = 15\,\mathrm{cm}$, $W = 15\,\mathrm{cm}$, $\epsilon_r = 6$, $\sigma = 0.001\,\mathrm{S/m}$. Inset image of (a) displays Gaussian transmitted pulse.

waveform that is a baseband Gaussian pulse with a bandwidth of $\Omega = 17.65\,\text{GHz}$ (note that a fractional bandwidth is not defined for a baseband pulse); this pulse is shown in the inset of Figure 2(a). Note that using a baseband pulse is an abstraction that cannot be realized practically, since the low frequency content of the system will be limited by the antenna impulse response. However, an equivalent large bandwidth will produce an equally excellent resolution of the scattering objects, as is seen in the figure. The first peak represents the reflection from the air/slab interface, and establishes the $t = 0$ time reference. The second peak is the reflection from the rear face of the slab, and the next two peaks are from multiple reflections within the slab. The reflection from the target is seen at 11 ns, and the following peaks represent multiple interactions between the target and the slab, which lead to the presence of "ghost" images. Note that the initial reflection (flash) from the front surface of the slab is nearly two orders of magnitude larger than the reflection from the target, and is cropped in Figure 2(a). The large flash presents dynamic range issues for the frequency-domain system since the flash and the target response are not separated. In a time-domain system, the initial reflection can be time gated out and the subsequent target reflection amplified separately from the flash.

Time-domain data were computed at 21 transmitter/receiver positions, equally spaced from $y = -2.5\,\text{m}$ to $y = 2.5\,\text{m}$ and are used to construct an image of the target. An observation region is created using a 2-dimensional rectangular grid, and the propagation time is calculated from each of the 21 different transmitter/receiver positions to each grid point. For simplicity, refraction at the air/barrier interface is ignored. The observation region extends from $y = -2.6\,\text{m}$ to $y = 2.6\,\text{m}$ and from $z = 0.5\,\text{m}$ to $z = -2.5\,\text{m}$, with a grid point spacing of 1 cm. Using the computed travel time, the strength of the total field is found from each time-domain waveform, and the results for each transmitter/receiver position are summed to determine the image intensity at each grid point. In this way a simple scattering center image is produced. Figure 2(b) displays the two-dimensional intensity image created within a grid that is chosen to include the conducting strip target and a portion of the barrier. Clearly visible in the image is the front of the barrier at $z = 0.15\,\text{m}$, and the rear of the barrier at $z = 0\,\text{m}$. Present, but difficult to see with the chosen scaling of the image intensity, is a ghost of the wall at $z = -0.15\,\text{m}$ produced by the multiple reflections within the wall. The target appears clearly at $z = -0.8\,\text{m}$.

The sharpness of the target image depends on the target SNR and the A/D bit length. To determine the effect of altering these

parameters, it is necessary to quantify the resolution of the target image. With knowledge of the target location for this parameter analysis, an image radius is defined representing the radius of a circle that has an area equal to the region that contains the majority of image intensity. An arbitrary box is taken around the target, with size large enough to contain the target but not too large so that other artifacts in the image are included. Inside the box, the center of grid point intensity (y_0, z_0) is determined using a formula akin to finding the center of mass of an object:

$$y_0 = \frac{\sum_{i=1}^{n_y} f_i y_i}{\sum_{i=1}^{n_y} y_i}, \quad z_0 = \frac{\sum_{i=1}^{n_z} f_i z_i}{\sum_{i=1}^{n_z} z_i}. \tag{11}$$

Here (y_i, z_i) is the grid point position, f_i is the intensity of the ith grid point, n_y is the number of grid points in the y-direction, and n_z is the number of grid points in the z-direction. The radius of intensity, R, is then found using

$$R = \frac{\sum_{i=1}^{n_y n_z} r_i \tau(f_i)}{\sum_{i=1}^{n_y n_z} \tau(f_i)}. \tag{12}$$

Here $r_i = [(y_i - y_0)^2 + (z_i - z_0)^2]^{1/2}$ and $\tau(f_i)$ is the thresholding function

$$\tau(f_i) = \begin{cases} f_i, & f_i > c \cdot \max_i\{f_i\} \\ 0, & f_i \leq c \cdot \max_i\{f_i\} \end{cases}, \tag{13}$$

where $c \in [0, 1]$. Thus, only those grid points with intensity greater than a chosen fraction of the maximal image intensity are used to compute R. Numerical experimentation has shown that a value of $c = 0.5$ produces good results and therefore is used in all examples shown here.

The image radius gives a measure of the sharpness of the image. A large image radius corresponds to a blurry image and a small radius to a sharper image.

4. PARAMETER ANALYSIS

To build a prototype stepped-frequency or short-pulse radar, it is necessary to settle on the values of certain parameters such as transmitted pulse width, sampling interval, SNR, and digitization level. Since the goal is to create an image of an object behind a barrier, the canonical problem described in Section 2 is used to determine the appropriate ranges of parameter settings that provide acceptable radar imaging performance. Simulated data sets were computed at 21 different transmitter/receiver positions equally spaced from $y =$

$-2.5\,\mathrm{m}$ to $y = 2.5\,\mathrm{m}$, images were created for different parameter sets, and the sharpness of each image was analyzed by computing the image radius.

4.1. Time-domain (Short-pulse) System

Appropriate canonical problem data were computed in the frequency domain and converted into time-domain data using the FFT. To avoid inaccuracies in the conversion process, a much smaller frequency sampling interval of 20 MHz was used when computing the data than is needed in the parameter analysis. The received pulse is baseband, with a width defined as the half-amplitude width of the widowing function from (9).

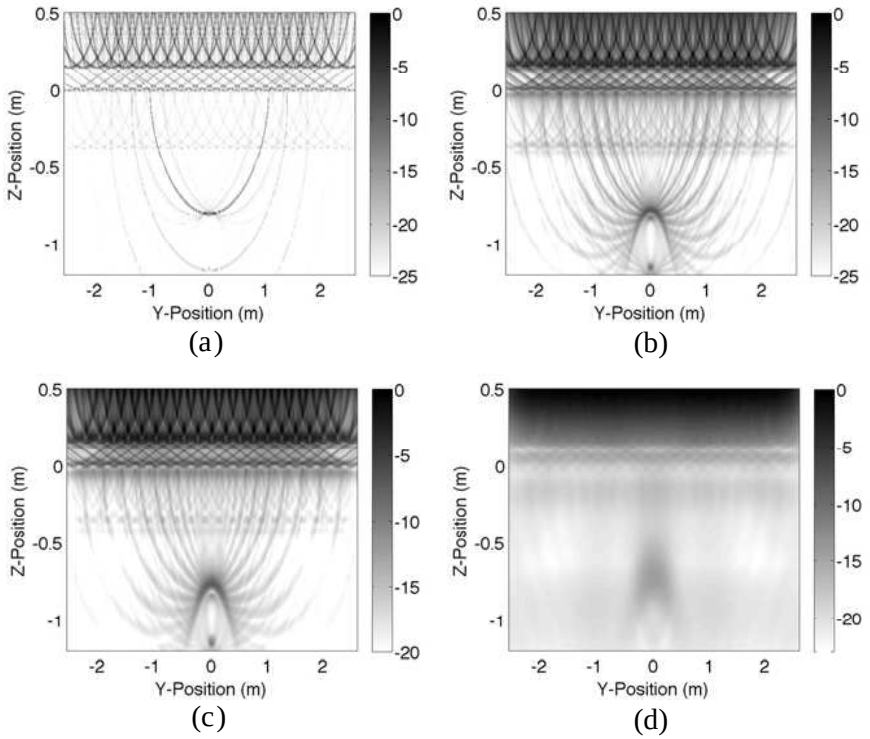

Figure 3. Conducting strip image (scale in dB) constructed using a pulse width of (a) $T = 0.05\,\mathrm{ns}$, (b) $T = 0.30\,\mathrm{ns}$, (c) $T = 0.50\,\mathrm{ns}$, (d) $T = 2.00\,\mathrm{ns}$. $z_s = 50\,\mathrm{cm}$, $z_t = 80\,\mathrm{cm}$, $z_w = 15\,\mathrm{cm}$, $W = 15\,\mathrm{cm}$, $\epsilon_r = 6$, $\sigma = 0.001\,\mathrm{S/m}$.

The parameters explored for a time-domain radar system include pulse width, sample rate, SNR, and digitization level. The received pulse width determines the equivalent bandwidth of the system. For the parameter analysis of the time-domain system, a set of baseline values was established and one parameter is varied in each study to determine its effect on image quality. The baseline values are a pulse width of $T = 0.10\,\text{ns}$, a sampling interval of 1.53 ps, zero noise added (SNR $= \infty$), and no artificial digitization of the data.

As seen in Figure 3, increasing the pulse width of the system causes a loss of resolution and thus the image of the target blurs and eventually fades into the background. Figure 4(a) shows the image radius values computed by centering a box of sides 30 cm tall by 46 cm wide on the target. It is clearly seen that increasing the pulse width enlarges the image radius, corresponding to a decrease in image quality.

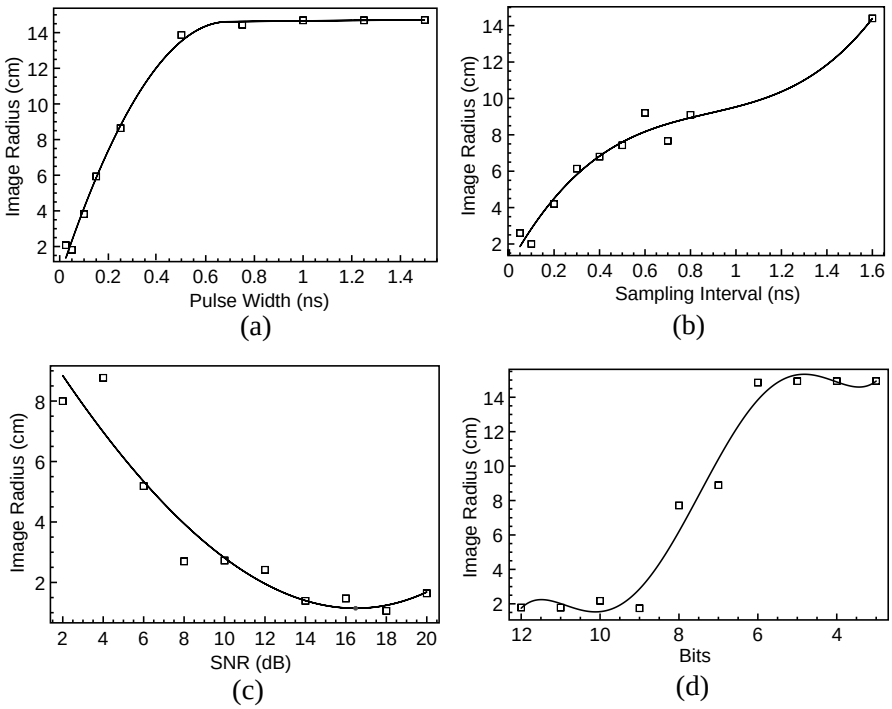

Figure 4. Effects on image radius generated by the time-domain system, due to (a) pulse width, (b) sampling interval, (c) SNR, (d) digitization. $z_s = 50\,\text{cm}$, $z_t = 80\,\text{cm}$, $z_w = 15\,\text{cm}$, $W = 15\,\text{cm}$, $\epsilon_r = 6$, $\sigma = 0.001\,\text{S/m}$. Line shows best fit trend.

Note that the image radius decreases between 0.06 ns and 0.10 ns. This is probably due to the choice of the threshold value, c, of the grid point intensity used to compute the image radius. A low value works well with wider pulses, but may not accurately predict the degradation of the image at narrow pulse widths.

The maximum usable pulse width depends on the desired resolution of the radar. It was found that when imaging a strip of width 15 cm an image radius of about 4 cm provides a usable localization of the image (note that image radius is not equivalent to strip width). Although this value is subjective, later analysis with multiple targets reveals that this image radius allows two strips to be resolved when separated by one strip width, and so also provides a convenient parameter for multiple target studies. Figure 4(a) indicates a pulse width of approximately 0.10 ns produces the desired 4 cm resolution.

Figure 4(b) shows the dependence of image radius on sampling interval. Here it is seen that the desired value of $R = 4$ cm occurs for a sampling interval of about 0.2 ns, which requires a minimum sampling rate of about 5 Gs/s. To determine the required SNR, white Gaussian noise was added directly in the time domain with a signal-to-noise ratio determined with reference to the largest peak in the waveform, which is the flash from the front of the barrier. Figure 4(c) shows the dependence of the image radius on SNR, suggesting that a minimum SNR of about 8 dB is required to produce an image radius of 4 cm. Finally, the dependence of image radius on amplitude digitization was explored by digitizing the time-domain signal with different A/D bit levels. From Figure 4(d) it is seen that at least 9 bits must be used to achieve an image radius of 4 cm. Using less bits produces a fairly dramatic increase in image radius. Note that the digitization was done assuming that the flash from the wall is present in the measured time-domain data. By setting the time reference of the receiver appropriately, the flash can be time-gated out and the required dynamic range can be decreased dramatically — hence fewer bits are required for the desired image quality.

The minimum required parameters identified from these simulations are summarized in Table 1.

Table 1. Minimum system requirements for a time-domain short-pulse radar system.

Pulse Width	Sampling Rate	SNR	Digitization
≤ 0.1 ns	≥ 5 Gs/s	≥ 8 dB	≥ 9 Bits

4.2. Frequency-domain (Stepped-frequency) System

Images for a frequency-domain system are created by using the simulated frequency-domain target data with constraints on the bandwidth, sampling interval, SNR, and A/D bit length. The constrained data are transformed into the time-domain using the FFT, and the same processing is applied as was used to form images for the time-domain system. The baseline parameter values for the frequency-domain system are a fractional bandwidth of 117.42%, a sampling interval of 20 MHz, zero added noise, and no digitization.

The bandwidth of the system determines the spatial resolution in much the same way that the pulse width does for a time-domain system. Figure 5(a) shows the image radius values computed for various percent bandwidths. To restrict the bandwidth of the simulated data, a fractional bandwidth Ω/f_0 was chosen and the equivalent temporal pulse width was calculated using (10). The value

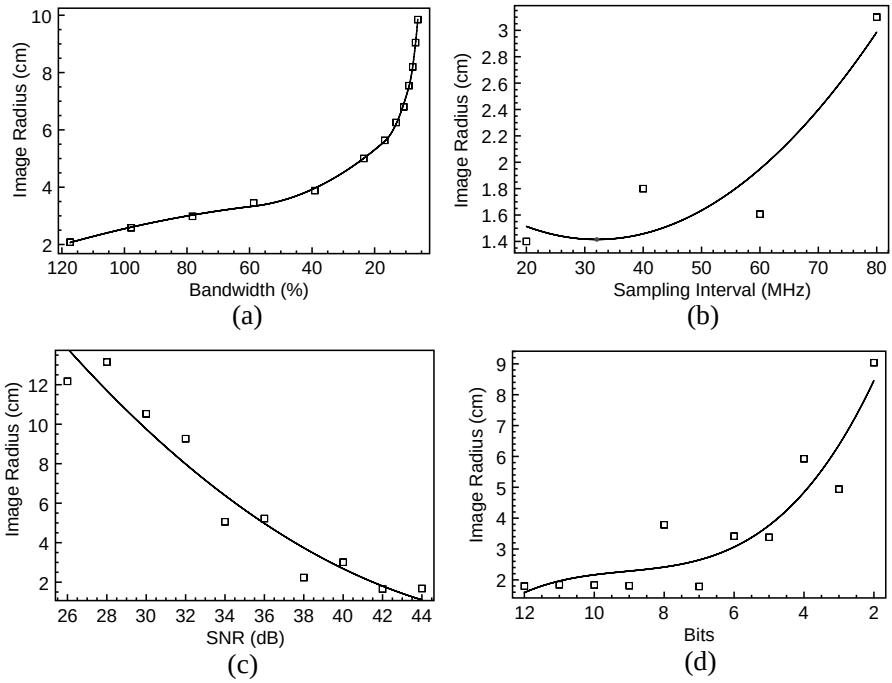

Figure 5. Effects on image radius generated by the frequency-domain system, due to (a) bandwidth, (b) sampling interval, (c) SNR, (d) digitization. $z_s = 50\,\text{cm}$, $z_t = 80\,\text{cm}$, $z_w = 15\,\text{cm}$, $W = 15\,\text{cm}$, $\epsilon_r = 6$, $\sigma = 0.001\,\text{S/m}$. Line shows best fit trend.

f_0 was chosen to be the center frequency of 8 GHz and the bandwidth was varied around this specific frequency. The data was then windowed using the function $W(f)$ in (9). As expected, the image radius increases as the bandwidth decreases, with a fractional bandwidth of about 37% required to produce an image radius no larger than 4 cm.

Figures 5(b)–5(d) show the effects of sampling interval, SNR, and discretization, respectively, on image radius. Figure 5(b) reveals that the image radius is not affected greatly by frequency sampling interval until a value of 80 MHz is reached. Beyond this point, aliasing creates overlapping images due to wraparound in the inverse FFT, and the image radius cannot be computed in a meaningful way. This provides a rigid upper limit on the requisite frequency sampling interval. The dependence of the image radius on SNR and digitization is as expected, with higher SNR and greater discretization required to produce better images. A summary of the minimum system parameters for a stepped-frequency system is provided in Table 2.

Table 2. Minimum system requirements for a frequency-domain radar system.

Fractional Bandwidth	Sampling interval	SNR	Digitization
$\geq 37\%$	≤ 40 MHz	≥ 40 dB	≥ 6 Bits

4.3. Multiple Target Resolution

Minimum system parameters more stringent than those identified in previous sections may be required to separate multiple targets. As a simple study, the field scattered by two adjacent conducting strips of the same width and varying separation was computed, and the associated images were generated. Figure 6 shows the images of two 15 cm wide strips formed using a pulse width of 0.10 ns, a sampling interval of 1.53 ps, zero noise added (SNR $= \infty$), and no artificial digitization of the data. With a strip separation of 5 cm (defined as the distance between adjacent strip edges), it is not possible to discern two targets. However with a separation of 50 cm, two images are clearly visible.

The minimum separation distance at which both targets can be resolved is determined by finding the distance at which the image radius, found using a box enclosing both conducting strips, approximately equals twice the image radius of a single strip, as found earlier. The size of the box surrounding the multiple targets was 30 cm tall and 162 cm wide. Figure 7 shows the two-strip image radius

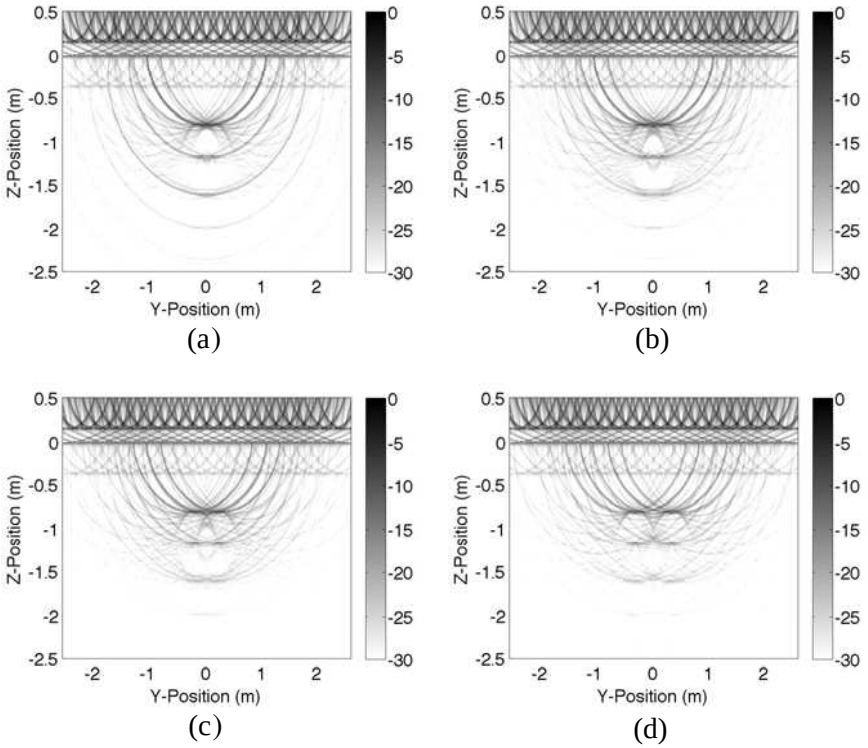

Figure 6. Images (scale in dB) of two conducting strips of width 15 cm constructed using a pulse width of 0.10 ns and a separation distance of: (a) 5 cm, (b) 15 cm, (c) 25 cm, (d) 50 cm. $z_s = 50$ cm, $z_t = 80$ cm, $z_w = 15$ cm, $\epsilon_r = 6$, $\sigma = 0.001$ S/m.

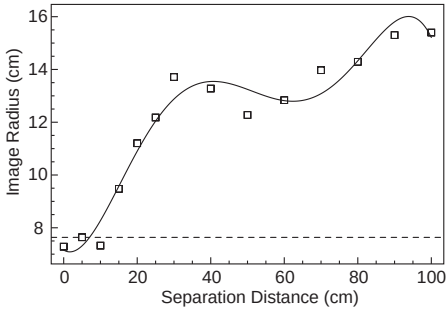

Figure 7. Image radius of two conducting strips of width 15 cm computed using a box that encloses both strips and a pulse width of 0.1 ns. Dashed line shows twice the image radius of a single strip. $h = 50$ cm, $z_s = 80$ cm, $t = 15$ cm, $\epsilon_r = 6$, $\sigma = 0.001 \frac{\mathrm{S}}{m}$. Solid line shows best fit trend.

as a function of separation distance, and indicates that a minimum separation distance of about 15 cm (one strip width) is needed for the two-strip image radius to be twice that of the single-strip radius of 3.8 cm.

An image radius of 4 cm was selected for the single-target parameter studies, in part, because two 15 cm wide strips can be resolved with this radius when the strips are separated by a distance equal to their width.

5. CONCLUSION

A two-dimensional canonical problem was studied to determine the effects of various radar parameters on the performance of short-pulse and stepped-frequency radar systems for imaging targets through barriers. The results provide a set of minimal requirements for producing acceptable target images, as defined using an image radius measure. Although the requirement on image radius is subjective and the minimum system parameters depend on the properties of both the target and the barrier, the parameters found in this study should provide a useful, general guide for designing both time and frequency-domain radar systems and for understanding the tradeoffs between the parameters.

The analysis demonstrates that both time-domain and short-pulse systems are generally capable of achieving similar performance. When considering the details of implementation, the primary difference between the systems deals with the required dynamic range and the fact that the short-pulse time-domain system can time gate out strong clutter signals, while the stepped-frequency system cannot. It is not well recognized that a frequency-domain system must accommodate the full range of the received frequencies, while a time-domain system can gate out the clutter — a considerable advantage. In fact, a significant amount of research for conventional radar has been devoted to overcoming this serious open problem of strong clutter obscuring smaller targets.

REFERENCES

1. Ahmad, F., G. Moeness, and G. Mandapati, "Autofocusing of through-the-wall radar imagery under unknown wall characteristics," *IEEE Trans. on Image Processing*, Vol. 16, No. 7, 1785–1795, Jul. 2007.
2. Baranoski, E. J., "Through-wall imaging: Historical perspective

and future directions," *Special Issue on Advances in Indoor Radar Imaging, J. Franklin Inst.*, 556–569, 2008.

3. Maaref, N., P. Millot, X. Ferrières, C. Pichot, and O. Picon, "Electromagnetic imaging method based on time reversal processing applied to through-the-wall target localization," *Progress In Electromagnetics Research M*, Vol. 1, 59–67, 2008.
4. Yang, Y. and A. E. Fathy, "See-through-wall imaging using ultra wideband short-pulse radar system," *IEEE Antennas and Propagation Society International*, 334–337, 2005.
5. Mokole, E. L. and P. Hansen, "Survey of ultra-wideband radar," *Ultra-wideband, Short-pulse Electromagnetics 7*, 571–585, 2007.
6. Hansen, P., K. Scheff, E. Mokole, and E. Tomas, "Dual frequency measurements of ocean forward scatter with an ultrawideband radar," *Proceedings of the 2001 IEEE Radar Conference*, 376381, Atlanta, GA, May 1–3, 2001.
7. Attiya, A. M., "UWB applications for through-wall detection," *IEEE Antennas Propag. Soc. Int. Symp.*, 3079–3082, 2004.
8. Taylor, J. D., *Introduction to Ultra-wideband Radar System*, CRC Press, 1995.
9. LaHaie, I. J., "Ultrawideband radar," *Proc. SPIE*, Vol. 1631, 1992.
10. Morgan, M. A., "Ultra-wideband impulse scattering measurements," *IEEE Trans. on Antennas and Propagation*, Vol. 42, No. 6, 840–846, Jun. 1994.
11. Falorni, P., L. Capineri, L. Masotti, and C. G. Windsor, "Analysis of time domain ultra-wide-band radar signals reflected by buried objects," *PIERS Online*, Vol. 3, No. 5, 662–665, 2007.
12. Kidera, S., T. Sakamoto, and T. Sato, "Experimental study of shadow region imaging algorithm with multiple scattered waves for UWB radars," *PIERS Online*, Vol. 5, No. 4, 393–396, 2009.
13. Vickers, R., "Ultrahigh resolution radar," *Proc. SPIE*, Vol. 1875, 1993.
14. Chen, F.-C. and W. C. Chew, "Time-domain ultra-wideband microwave imaging radar system," *Journal of Electromagnetic Waves and Applications*, Vol. 17, No. 2, 313–331, 2003.
15. Fontana, R. J., "Recent system applications of short-pulse ultra wideband (UWB) technology," *IEEE Trans. on Microwave Theory and Techniques*, Vol. 52, No. 9, 2087–2104, Sep. 2004.
16. Chan, Y. K. and V. C. Koo, "An introduction to synthetic aperture radar (SAR)," *Progress In Electromagnetics Research B*, Vol. 2, 27–60, 2008.
17. Chan, Y. K., V. C. Koo, and T. S. Lim, "Conceptual design of a

high resolution, low cost X-band airborne synthetic aperture radar system," *PIERS Online*, Vol. 3, No. 6, 943–947, 2007.

18. Mei, C., M. Hasanovic, J. K. Lee, and E. Arvas, "Electromagnetic scattering from an arbitrarily shaped three-dimensional inhomogeneous bianisotropic body," *PIERS Online*, Vol. 3, No. 5, 680–684, 2007.
19. Crowgey, B. R., "Comparison of UWB-pulse and stepped-frequency systems for imaging through barriers," Masters Thesis, Michigan State University, East Lansing, 2009.
20. Sabath, F., E. L. Mokole, and S. N. Samaddar, "Definition and classification of ultra-wideband signals and devices," *The Radio Science Bulletin*, No. 313, Jun. 2005.
21. Davis, J., Y. Huang, S. G. Millard, and J. H. Bungey, "Determination of dielectric properties of insitu concrete at radar frequencies," *International Symposium (NDT-CE 2003), Non-destructive Testing in Civil Engineering*, 2003.